Research Article

Perovskite Transparent Conducting Oxide for the Design of a Transparent, Flexible, and Self-Powered Perovskite Photodetector

Ruixing Xu, Liangliang Min, Zhimin Qi, Xiyuan Zhang, Jie Jian, Yanda Ji, Fengjiao Qian, Jiyu Fan, Caixia Kan, Haiyan Wang, Wei Tian, Liang Li, Weiwei Li,* and Hao Yang*

Cite This: *ACS Appl. Mater. Interfaces* 2020, 12, 16462−16468

Read Online

ACCESS | Metrics & More | Article Recommendations

ABSTRACT: Transparent and flexible electronic devices are highly desired to meet the great demand for next-generation devices that are lightweight, flexible, and portable. Transparent conducting oxides (TCOs), such as indium-tin oxide, serve as fundamental components for the design of transparent and flexible electronic devices. However, indium is rare and expensive. Herein, we report the fabrication of low-cost perovskite $SrVO_3$ TCO films on transparent and flexible mica substrates and further demonstrate their utilization as a TCO electrode for building a transparent, flexible, and self-powered perovskite photodetector. Superior stable optical transparency and electrical conductivity are retained in $SrVO_3$ after bending up to 10^5 cycles. Without an external power source, the constructed all-perovskite photodetector exhibits a high responsivity (42.5 mA W^{-1}), fast response time (3.09/1.23 ms), and an excellent flexibility and bending stability after dozens of cycles of bending at an extreme 90° bending angle. Our results demonstrate that low-cost and structure-compatible transition metal-based perovskite oxides, such as $SrVO_3$, as TCO electrodes have huge potential for building high-performance transparent, flexible, and portable smart electronics.

KEYWORDS: *transparent conducting oxides, SrVO₃, perovskite, self-powered photodetector, flexible*
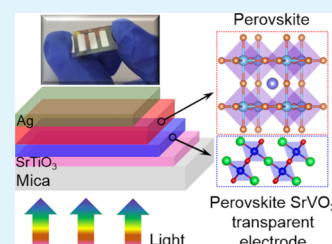
1. INTRODUCTION

Transparent flexible devices, including photodetectors,[1,2] transistors,[3−5] sensors,[6−8] nonvolatile memristors,[9−11] and displays,[12,13] have been widely studied for meeting the great demands of next-generation smart electronics. Transparent conducting oxides (TCOs) that combine visible-range optical transparency and electrical conductivity serve as fundamental components (*e.g.*, electrode elements and structural templates) in the design and fabrication of these optoelectronic devices.[14−17] Up to now, the commercially available electronics, such as photodetectors, photovoltaics, solar cells, and flat panel displays, are mostly constructed on indium-tin oxide (ITO)-coated polymer substrates owing to its unique combination of optical transparency, electrical conductivity, and ease of fabrication.[14,18−21] However, indium is rare and expensive. Moreover, the ITO-coated substrates are fragile and not resistant to high temperature. Considering the rapid development of perovskite-based photovoltaics and photodetectors, indium-free and low-cost TCOs with structural compatibility, similar to perovskites, are highly desired to explore.

Perovskite oxides have attracted intensive research interests because of their fascinating physical properties.[22−24] Recently, because of the cost-efficient and intrinsically metallic property, early transition metal-based perovskite oxides with partially filled d orbitals have been widely investigated as new TCOs, which electrical conductivity and optical transparency can be

optimized by the electron effective mass $m*$ simultaneously.[16,17,25−27] Additionally, the electron mean free path in these transition metal oxides is short (<10 nm) and comparable to that of ITO. In turn, the less free carrier reflection, high flexibility, and conductivity of thinner films can be maintained as same as that of thicker films. Perovskite $SrVO_3$ (SVO) was identified to be a new promising TCO electrode. The demonstrated properties of SVO films grown on unbendable or rigid substrates, such as carrier concentration (2.0 to 2.6×10^{22} cm^{-3}), room-temperature conductivity (1.6 to 3.5×10^4 S cm^{-1}), room-temperature carrier mobility (5−10 cm^2 V^{-1} s^{-1}), and wavelength-averaged transmissions in the visible range (>60%), stand up to those of the standard ITO films, providing therefore a valuable alternative for a wide range of applications.[25,28−30] Unfortunately, few reports are devoted to the fabrication of flexible SVO films. Further, it is still an open question whether perovskite SVO (or other early transition metal-based) TCO films can be integrated for the design and construction of high performance, transparent, and flexible optoelectronic devices, such as photodetector.
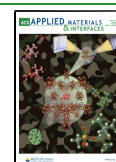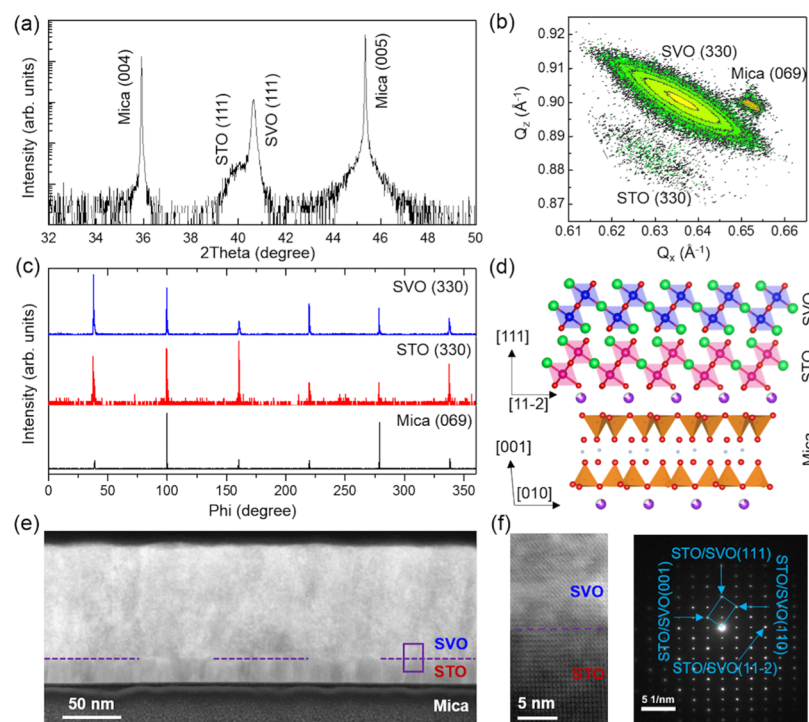
Figure 1. (a) Typical XRD $\theta-2\theta$ scan of SVO/STO/mica. (b) RSM of (069) and (330) Brag reflections of mica and SVO/STO, respectively. (c) ϕ-scans of SVO (330), STO (330), and mica (069). (d) Crystallographic model of the SVO/STO and STO/mica interfaces. (e) Cross-section STEM image showing the SVO and STO layer, and also the mica substrate. (f) Left panel: high-resolution TEM image of the SVO and STO interface, corresponding to the rectangle region in (e). Right panel: selected area diffraction pattern indicating the high quality epitaxial growth of the SVO film.

Transparent flexible photodetectors that capture light signals and convert them into electric signals have attracted immense research interests because of their great promise in next-generation lightweight, portable, and wearable optoelectronic devices. Owing to their excellent semiconductor properties, such as a direct band gap, a broad absorption range, high carrier mobility, low excitation binding energies, and a long carrier diffusion length,[31−35] hybrid organic−inorganic perovskites have been promising candidates for high-performance transparent and flexible photodetectors. However, one of the issues limiting the application of transparent and flexible perovskite photodetectors is that they usually require an external power supply to separate the photoexcited electron−hole pairs, which increases the device cost and weight.[36,37] It is urgent but challenging to design and construct transparent and flexible perovskite photodetectors with the self-powering capability.

In this work, for the first time, we report a self-powered, transparent, and flexible photodetector consisting of a structure-compatible perovskite SVO TCO electrode and a high performance $Cs_{0.05}(FA_{0.85}MA_{0.15})_{0.95}Pb(I_{0.85}Br_{0.15})_3$ perovskite film. High-quality epitaxial SVO films with excellent mechanical flexibility were grown on $SrTiO_3$ (STO)-buffered fluorphlogopite [mica, $KMg_3(AlSi_3O_{10})F_2$] substrates. Superior stable optical transparency (an average visible transmittance of 53−67% for a 40 nm SVO film) and electrical conductivity (2.33×10^{-4} $\Omega\cdot cm$) can be maintained by bending with different curvatures and up to 10^5 bending cycles. We further demonstrate an integrated self-powered all-perovskite photodetector, which exhibits a high responsivity (42.5 mA W^{-1}) and fast response time (3.09/1.23 ms) at a wavelength of 532 nm. Moreover, the device shows an outstanding stability after a

long-term photoresponse measurement (5 h). Furthermore, the excellent flexibility and stability were also presented by performing various bending cycles at an extreme 90° bending angle. These critical parameters are comparable to and even better than those of the previously reported perovskite photodetectors based on ITO TCO films. Our results demonstrate a huge potential for building high-performance, transparent, flexible, and self-powered perovskite photodetectors by using indium-free, cost-efficient, perovskite-type TCO films.

2. RESULTS AND DISCUSSION

2.1. Epitaxial Growth and Crystallographic Analyses. We first used pulsed laser deposition with sintered SVO and STO targets to synthesize high-quality SVO films with a STO buffer layer. Figure 1a shows X-ray diffraction (XRD) $\theta-2\theta$ scan of the SVO/STO/mica heterostructure revealing that the film is epitaxial and single-phased, confirming no intermixed crystalline phases. Based on the SVO peak position, the out-of-plane lattice constant is calculated to be 2.218 ± 0.003 Å, consistent with the lattice constant of bulk,[25] indicating that the strain caused by the lattice mismatch between the film and the mica substrate is fully relaxed. This is further confirmed by the X-ray reciprocal space map (RSM), as shown in Figure 1b, and also can be understood by the very weak interaction between the film and mica substrate due to the nature of van der Waals epitaxy.[11,24] In addition, the in-plane structural relationships are obtained by analyzing the phi-scan results of SVO (330), STO (330), and mica (069) diffraction peaks (Figure 1c). The six-fold symmetry of SVO (330) and STO (330) could be explained by the formation of multidomains. A schematic of SVO/STO bilayer films grown on mica with the

determined orientation relationship, SVO[111]‖STO[111]‖ mica[001] and SVO[11 − 2]‖STO[11 − 2]‖mica[010], is constructed and shown in Figure 1d. The microstructure of the SVO/STO/mica heterostructure was further investigated by scanning transmission electron microscopy (STEM), as shown in Figure 1e,f. The cross-sectional STEM images reveal the layer structure of the SVO/STO/mica heterostructure and also exhibit the defect-free at the interfaces of SVO/STO and STO/mica in the heterostructure. Because of the small lattice mismatch between STO (d_{111} = 2.253 Å, PDF#42-0734) and SVO (d_{111} = 2.217 Å, PDF#42-0039), the coherent interface is formed between SVO and STO. As a consequence, the strain at the interface causes the overlapped diffraction dots at a local SVO/STO region, as shown in the right panel of Figure 1f.

2.2. Transport Property. In the view of SVO-based flexible optoelectronic applications, the operational stability and mechanically durability of the SVO/STO/mica heterostructure were tested under both the flex-in mode (the film is under compressive strain) and the flex-out mode (the film is under tensile strain). Figure 2a shows that the values of R/R_0
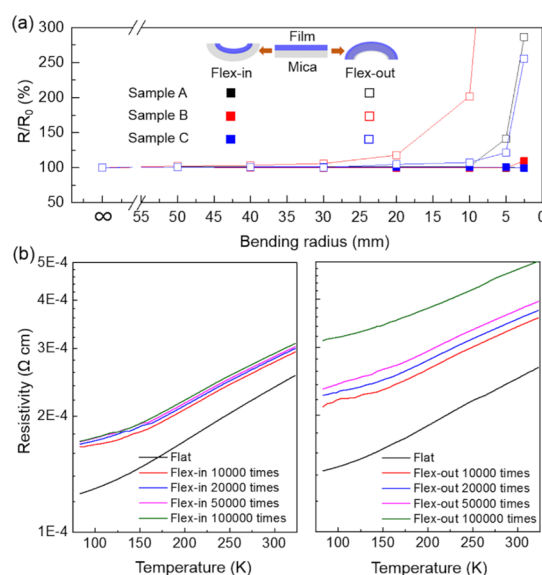

Figure 2. (a) Ratio of resistance as a function of bending radius of curvature under flex-in (filled squares) and flex-out (open squares) modes for three different SVO samples with the same thickness of 40 nm. R is the resistance with bending, and R_0 is the resistance without bending. (b) Temperature-dependent resistivity of the bending radius of curvature 10 mm under flex-in (left panel, compressive strain) and flex-out (right panel, tensile strain) modes for the 40 nm SVO film.

(R_0 is the sheet resistance of the flat film, R is the sheet resistance of the bending film) remain approximately constant under a bending radius of 5 mm during both the compressive and tensile deformations, respectively, for SVO indicating the robustness of epitaxial SVO/STO/mica under bending for flexible device applications. We also found that the SVO film exhibits excellent flexibility in the flex-in mode. Especially, the sheet resistance approximately remains constant under the bending radius of >2 mm. There is a slight increase of ~3.1% in the sheet resistance when the bending radius reaches 2 mm. In sharp contrast to the flex-in mode, the sheet resistance in the flex-out mode is greatly increased by multiplication, starting at a bending radius of 5 mm. This is because the cracks caused by tensile strain are showing up on the SVO film's

surface. These results demonstrate that the mica substrates can maintain the macroscopic integrity of the SVO film in the flex-in mode. Furthermore, the resistivity stability of the SVO film as a function of bending cycles in the flex-in and flex-out modes was examined and shown in Figure 2b,c. After 1×10^4 bending cycles, there is an increase of 15.09 and 34.56% in the resistivity for the flex-in and flex-out modes, respectively. Note that the increase rate of resistivity is very slow after 1×10^4 bending cycles, and the resistivity remains almost same within 1×10^5 and 5×10^4 bending cycles for the flex-in and flex-out modes, respectively. We also observed that there is a clear increase of resistivity in the flex-out mode after 1×10^5 bending cycles. It is noteworthy that the resistivity of the SVO film after bending under the flex-in or flex-out mode is still comparable to that of the SVO film grown on unbendable substrates.[25,29,30] Therefore, the SVO film as the TCO electrode of flexible optoelectronic devices retains an outstanding stability of electrical conductivity after bending under a radius of curvature 5 mm.

2.3. Optical Property. Figure 3a shows the thickness-dependent optical transmittance spectra of epitaxial SVO/STO/mica films in the ultraviolet−visible−infrared regime. Photographs of the films with different thicknesses on a colored background are also shown as an inset. We can see that the bare mica substrate exhibits extraordinary transmittance in the whole measured range without any sharp absorption features, and the transmittance of SVO/STO/mica films decreases at the wavelength near 400 nm, originating from the STO buffer layer intraband transition located at around 3.2 eV.[38,39] On this transparent mica substrate, we obtained an average visible transmittance of 53−67% for 40 nm the SVO film. We also note that the visible transmittance is rapidly decreasing with the increase of the SVO film thickness. The stability of optical transparency was further examined by bending in the flex-out mode under a radius of curvature of 5 mm (Figure 3b). We observed the superior stability of transmittance with the same values after bending up to 1×10^5. This indicates that the perovskite SVO film has an excellent mechanical stability and provides huge potential for the application of transparency and flexible optoelectronic devices.

2.4. Perovskite Photodetector Activities. Given the above discussion and results, we constructed a perovskite detector consisting of the TCO electrode of the perovskite 40 nm SVO film (high visible transmittance and low sheet resistance) and a high-performance $Cs_{0.05}(FA_{0.85}MA_{0.15})_{0.95}Pb$-$(I_{0.85}Br_{0.15})_3$ perovskite film. Figure 4a shows the photograph of a real photodetector (top panel) and a schematic illustration of the device structure (bottom panel). Basically, the SVO layer serves as the light transmission window and top electrode, and also the structure of SVO is compatible with the perovskite. The corresponding energy level of each layer is shown in Figure 4b.[40] Because of such suitable energy levels, effectively transferring electrons and holes can be achieved. Figure 4c shows the time-dependent current ($I−t$) curves of the perovskite detector illuminated by 365, 532, 650, and 750 nm light at 0 V. As the pulsed beam is shining or off, the photocurrent is immediately generated or vanished, respectively, without requiring an extra power supply. The highest photocurrent was obtained at 532 nm, which is the same to the wavelength of the highest transmittance observed in the SVO film (Figure 3a). Response speed is a critical parameter of photodetectors, which is measured using an oscilloscope (Figure 4d). The rise time (the time taken for the response
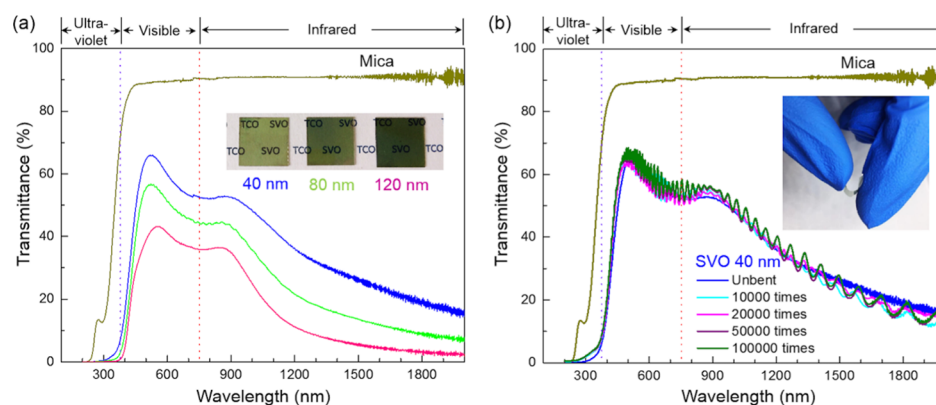
Figure 3. (a) Optical transmittance spectra of SVO films with varying thickness on the mica substrate. The inset shows the photographs of SVO films with different thicknesses. (b) Optical transmittance spectrum of a 40 nm SVO film with different bending cycles under a radius of curvature of 5 mm (flex-out mode). The inset shows a photograph of the 40 nm SVO film with bending.
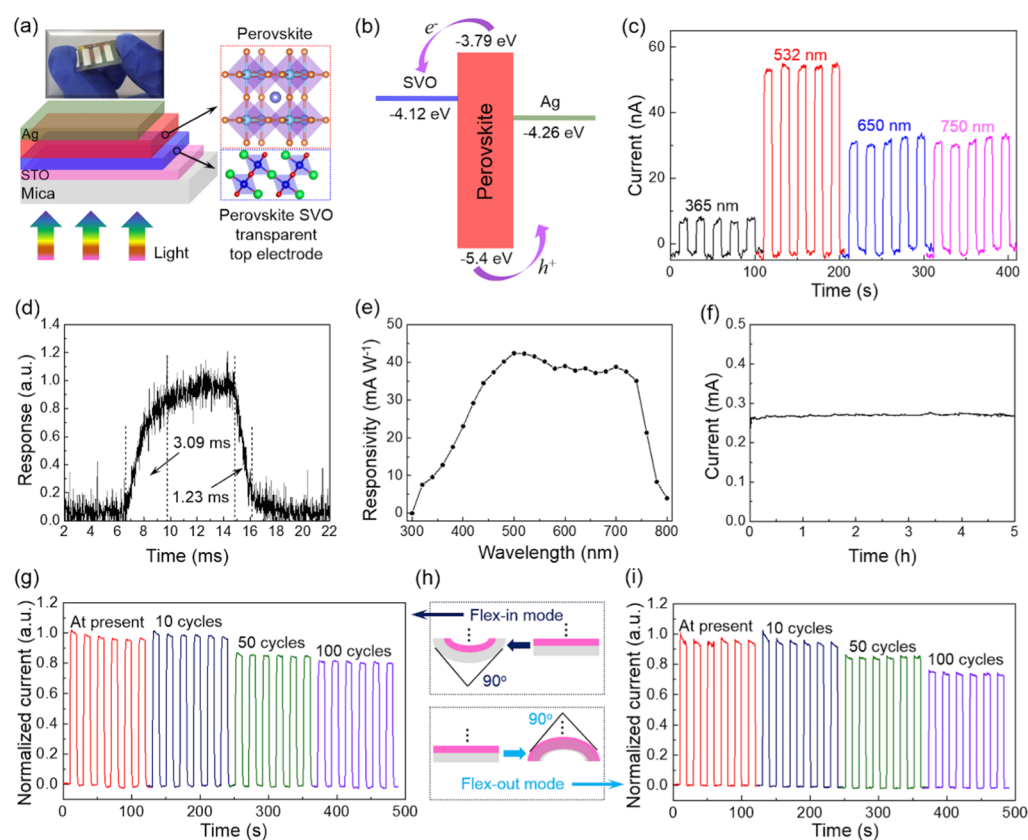

Figure 4. (a) Top panel is the photograph of a photodetector device. The bottom panel is a schematic illustration of the device structure. (b) Energy-level diagram of the photodetector device. (c) $I-t$ curves of the photodetector device under different wavelengths of light illumination at 0 V. (d) Response speed, (e) responsivity, and (f) long-term photoresponse curves of the photodetector device. $I-t$ curves at the angle of 90° under different bending cycles using (g) flex-in mode [top panel in (h)] and (i) flex-out mode [bottom panel in (h)] at 0 V.

increasing from 10 to 90% of the maximum value) and the decay time (the time taken for the response decreasing from 90 to 10% of the maximum value) are determined to be 3.09 and 1.23 ms, respectively, verifying the faster response speed for the perovskite photodetector based on the TCO electrode of the perovskite SVO film.

To quantify the wavelength selectivity of devices, the spectral responsivity (R) was measured at 0 V bias (Figure 4e). R is calculated with $R = (I_{on} - I_{off})/P_{in}$, where I_{on} is the photocurrent, I_{off} is the dark current, and P_{in} is the incident light power. R is above 20 mA W^{-1} in the visible range from

400 to 750 nm, with a peak value of 42.5 mA W^{-1} at a wavelength of 500 nm. These critical parameters are comparable to and even higher than the previously reported semitransparent/transparent perovskite photodetectors (Table 1). Stability is a key parameter for the practical application, so the long-term photoresponse measurement was performed and is shown in Figure 4f. The photocurrent of the perovskite detector is super stable, and no visible degradation is observed after subjecting it to white light for 5 h. The bending stability of the device is also characterized to demonstrate its promising utilization in wearable electronics. The definition of the 90°

Table 1. Comparison of the Critical Parameters for Semitransparent/Transparent Photodetectors

devices	film/TCO	flexible/self-power	light [nm]	rise/decay time	responsivity [A W^{-1}]	refs
$Cs_{0.05}(FA_{0.85}MA_{0.15})_{0.95}Pb(I_{0.85}Br_{0.15})_3$	Y/SVO	Y/Y	532	3.09/1.23 ms	0.0425	this work
$CH_3NH_3PbI_3$	N/null	Y/N	650	500/500 ms	0.1	36
$CH_3NH_3PbI_3$	Y/ITO	Y/N	459	50/120 μs	0.004	42
$CH_3NH_3PbI_3$	Y/ITO	Y/N	365	<0.2 s	3.49	37
			780	<0.1 s	0.037	
$CH_3NH_3PbI_3$	N/null	N/N	650	0.2/0.3 ms	0.85	43
$CH_3NH_3PbI_3$	Y/ITO	N/N	532	10/5.7 μs	242	44
$CH_3NH_3PbI_3$	Y/ITO	Y/Y	550	2200/300 ms	0.03	45
$MAPbCl_3$	Y/ITO	N/N	385	1 ms	18	46
$MAPbCl_3$	Y/Pt	N/N	365	24/62 ms	0.047	47
$MAPbBr_3$	Y/ITO	N/N	450	25 μs	4000	48
$CsPbBr_3$:ZnO	Y/ITO	N/Y	365	409/17.92 ms	0.0115	49
$CH_3NH_3PbI_3$	Y/ITO	Y/Y	simulated sunlight	80/80 ms	0.418	50
$CH_3NH_3PbI_3$	Y/AuNW	Y/Y	630	4.0/3.3 μs	0.314	51
$FA_{1-x}Cs_xPb(I_{1-y}Br_y)_3$	Y/null	Y/N	450	108/347 μs	5.0	52
$P(VDF-TrFE)/CH_3NH_3PbI_3$	N/null	Y/Y	650	88/154 μs	0.012	53

bending angle in the flex-in and flex-out modes is shown in Figure 4h. The bending performance of the device was tested at 0 V bias. As shown in Figure 4g,i, after 100 cycles of bending at an extreme 90 degree bending angle under both the flex-in and flex-out modes, the time-dependent photoresponse curves still exhibit fast response speed and have reproducible characteristics under periodic light illumination. These results strongly suggest the excellent flexibility and stability of the self-powered perovskite photodetector based on the TCO electrode of the perovskite SVO film.

3. CONCLUSIONS

In conclusion, we have fabricated high-quality epitaxial perovskite SVO TCO films on transparent and flexible mica substrates by pulsed laser deposition and further demonstrated its utilization as a low-cost and structure-compatible TCO electrode for constructing a transparent, flexible, and self-powered hybrid organic–inorganic perovskite photodetector. Perovskite SVO TCO films retain excellent performance of optical transparency and electrical conductivity after bending with different curvatures and up to 10^5 bending cycles. A self-powered all-perovskite photodetector is built and exhibits high responsivity (42.5 mA W^{-1}) and fast response time (3.09/1.23 ms) at a wavelength of 532 nm. Furthermore, a superior stability without any visible degradation is also demonstrated by a long-term photoresponse measurement (5 h). The device also shows excellent flexible performance when subjected to dozens of cycles of bending at an extreme 90° bending angle, possessing fast response speed and reproducible photoresponse. This work demonstrates that the perovskite SVO TCO electrode is a promising candidate for the commercial application of designing high-performance transparent, flexible, and wearable optoelectronic devices.

4. EXPERIMENTAL DETAILS

4.1. Film Fabrication. Epitaxial SrVO$_3$ films were grown on mica substrates using pulsed laser deposition using a KrF laser (λ = 248 nm) with a fluence of 3 J·cm^{-2} and a repetition rate of 2 Hz. During deposition, the substrate temperature was set at 630 °C and the oxygen partial pressure was fixed at 1×10^{-4} mbar. Prior to the growth of SrVO$_3$, a STO buffer layer was deposited at a substrate temperature of 630 °C under an oxygen partial pressure of 0.05 mbar. The thin films were further *ex situ* postannealed at 780 °C under a flowing gas of 95 vol % Ar + 5 vol % H$_2$ for 2 h.

4.2. Basic Characterization. The crystalline nature of the films was investigated by XRD on a high-resolution X-ray diffractometer (Panalytical Empyrean) using Cu K$_\alpha$ radiation (λ = 1.5406 Å). Transmission electron microscopy (TEM, FEI TALOS 200X operated at 200 kV) was used to investigate the microstructure of the film. The surface morphology was investigated by atomic force microscopy (Asylum Research MFP-3D-SA).

4.3. Transport and Optical Measurements. Transport properties were measured by Keysight B2902A using the standard four-probe method and the temperature range of 170−330 K was controlled by Linkam LNP95. Optical properties were investigated using SHIMADZU UV-3600 plus within the wavelength range of 200−2500 nm.

4.4. Fabrication of Self-Powered Photodetector. To fabricate photodetector devices, 0.531 g PbI$_2$, 0.1875 g FAI, 0.0734 g PbBr$_2$, and 0.0224 g of MABr were dissolved in the mixed solvent of dimethylformamide/dimethyl sulfoxide (DMSO) (375/585 μL). Then, 40 μL of CsI/DMSO solution (390 mg/mL) was added into the above solution, and the precursor solution was stirred at 343 K for 15 min before use. After that 50 μL of the precursor solution was spin-coated on the SVO film at 1000 rpm for 10 s and 4000 rpm for 35 s. Chlorobenzene (100 μL) was dropped 10 s before the end of spin-coating as antisolvent. Also, the device was placed on a hot stage to anneal at 373 K for 10 min, followed by the evaporation of a 90 nm Ag electrode.[41]

4.5. Photoelectrical Measurements. Time-dependent current ($I−T$) curves were collected by a semiconductor characterization system (Keithley 4200), along with monochromatic (Zolix, Omni-λ 3009) order sorting filters to produce monochromatic light. The response time was measured using an oscilloscope (MSO58, Tektronix) under a 532 nm laser of 128.8 Hz. The long-time stability was measured under a light-emitting diode light of 0.6 mA W^{-1}, with a humidity of 40% at room temperature. In the bending test, the device was measured in the initial state after different bending cycles at the angle of 90° under the flex-in and flex-out modes.

■ AUTHOR INFORMATION

Corresponding Authors

Weiwei Li — *Department of Materials Science & Metallurgy, University of Cambridge, Cambridge CB3 0FS, U.K.;* orcid.org/0000-0001-5781-5401; Email: wl337@cam.ac.uk

Hao Yang — *College of Science and Key Laboratory for Intelligent Nano Materials and Devices of the Ministry of Education, Nanjing University of Aeronautics and Astronautics, Nanjing 211106, P. R. China;* Email: yanghao@nuaa.edu.cn

Authors

Ruixing Xu − *College of Science, Nanjing University of Aeronautics and Astronautics, Nanjing 211106, P. R. China*

Liangliang Min − *School of Physical Science and Technology, Jiangsu Key Laboratory of Thin Films, Soochow University, Suzhou 215006, P. R.China*

Zhimin Qi − *School of Materials Engineering, Purdue University, West Lafayette, Indiana 47907, United States*

Xiyuan Zhang − *College of Science, Nanjing University of Aeronautics and Astronautics, Nanjing 211106, P. R. China*

Jie Jian − *School of Materials Engineering, Purdue University, West Lafayette, Indiana 47907, United States*

Yanda Ji − *College of Science, Nanjing University of Aeronautics and Astronautics, Nanjing 211106, P. R. China*

Fengjiao Qian − *College of Science, Nanjing University of Aeronautics and Astronautics, Nanjing 211106, P. R. China*

Jiyu Fan − *College of Science, Nanjing University of Aeronautics and Astronautics, Nanjing 211106, P. R. China;* orcid.org/0000-0001-6698-6384

Caixia Kan − *College of Science, Nanjing University of Aeronautics and Astronautics, Nanjing 211106, P. R. China;* orcid.org/0000-0003-3722-422X

Haiyan Wang − *School of Materials Engineering, Purdue University, West Lafayette, Indiana 47907, United States;* orcid.org/0000-0002-7397-1209

Wei Tian − *School of Physical Science and Technology, Jiangsu Key Laboratory of Thin Films, Soochow University, Suzhou 215006, P. R.China;* orcid.org/0000-0001-8941-6288

Liang Li − *School of Physical Science and Technology, Jiangsu Key Laboratory of Thin Films, Soochow University, Suzhou 215006, P. R.China;* orcid.org/0000-0003-0708-7762

Complete contact information is available at:
https://pubs.acs.org/10.1021/acsami.0c01298

Author Contributions

H.Y. and W.L. supervise the project. R.X. fabricated the samples and carried out XRD, optical and transport measurements with the support from X.Z., Y.J., F.Q., J.F., and C.K. Z.Q., J.J., and H.W. performed the TEM measurement. L.M., W.T. and L.L. conducted photoelectrical measurements. R.X., W.L. and H.Y. prepared the manuscript with the contribution from all authors.

Notes

The authors declare no competing financial interest.

■ REFERENCES

(1) Nomura, K.; Ohta, H.; Takagi, A.; Kamiya, T.; Hirano, M.; Hosono, H. Room-Temperature Fabrication of Transparent Flexible Thin-Film Transistors Using Amorphous Oxide Semiconductors. *Nature* **2004**, *432*, 488.

(2) Sekitani, T.; Nakajima, H.; Maeda, H.; Fukushima, T.; Aida, T.; Hata, K.; Someya, T. Stretchable Active-Matrix Organic Light-Emitting Diode Display Using Printable Elastic Conductors. *Nat. Mater.* **2009**, *8*, 494.

(3) Ju, S.; Facchetti, A.; Xuan, Y.; Liu, J.; Ishikawa, F.; Ye, P.; Zhou, C.; Marks, T. J.; Janes, D. B. Fabrication of Fully Transparent Nanowire Transistors forTransparent and Flexible Electronics. *Nat. Nanotechnol.* **2007**, *2*, 378.

(4) Eda, G.; Fanchini, G.; Chhowalla, M. Large-Area Ultrathin Films of Reduced Graphene Oxide as A Transparent and Flexible Electronic Material. *Nat. Nanotechnol.* **2008**, *3*, 270.

(5) Georgiou, T.; Jalil, R.; Belle, B. D.; Britnell, L.; Gorbachev, R. V.; Morozov, S. V.; Kim, Y.-J.; Gholinia, A.; Haigh, S. J.; Makarovsky, O.; Eaves, L.; Ponomarenko, L. A.; Geim, A. K.; Novoselov, K. S.; Mishchenko, A. Vertical Field-Effect Transistor Based on Graphene−WS₂ Heterostructures for Flexible and Transparent Electronics. *Nat. Nanotechnol.* **2013**, *8*, 100.

(6) Segev-bar, M.; Haick, H. Flexible Sensors Based on Nanoparticles. *ACS Nano* **2013**, *7*, 8366.

(7) Wang, Q.; Jian, M.; Wang, C.; Zhang, Y. Carbonized Silk Nanofiber Membrane for Transparent and Sensitive Electronic Skin. *Adv. Funct. Mater.* **2017**, *27*, 1605657.

(8) Sarwar, M. S.; Dobashi, Y.; Preston, C.; Wyss, J. K. M.; Mirabbasi, S.; Madden, J. D. W. Bend, Stretch, and Touch: Locating a Finger on An Actively Deformed Transparent Sensor array. *Sci. Adv.* **2017**, *3*, No. e1602200.

(9) Kim, K. L.; Lee, W.; Hwang, S. K.; Joo, S. H.; Cho, S. M.; Song, G.; Cho, S. H.; Jeong, B.; Hwang, I.; Ahn, J.-H.; Yu, Y.-J.; Shin, T. J.; Kwak, S. K.; Kang, S. J.; Park, C. Epitaxial Growth of Thin Ferroelectric Polymer Films on Graphene Layer for Fully Transparent and Flexible Nonvolatile Memory. *Nano Lett.* **2016**, *16*, 334.

(10) Qian, K.; Tay, R. Y.; Lin, M.-F.; Chen, J.; Li, H.; Lin, J.; Wang, J.; Cai, G.; Nguyen, V. C.; Teo, E. H. T.; Chen, T.; Lee, P. S. Direct Observation of Indium Conductive Filaments in Transparent, Flexible, and Transferable Resistive Switching Memory. *ACS Nano* **2017**, *11*, 1712.

(11) Le, V.-Q.; Do, T.-H.; Retamal, J. R. D.; Shao, P.-W.; Lai, Y.-H.; Wu, W.-W.; He, J.-H.; Chueh, Y.-L.; Chu, Y.-H. Van der Waals Heteroepitaxial AZO/NiO/AZO/Muscovite (ANA/muscovite) Transparent Flexible Memristor. *Nano Energy* **2019**, *56*, 322.

(12) Zhang, D.; Ryu, K.; Liu, X.; Polikarpov, E.; Ly, J.; Tompson, M. E.; Zhou, C. Transparent, Conductive, and Flexible Carbon Nanotube Films and Their Application in Organic Light-Emitting Diodes. *Nano Lett.* **2006**, *6*, 1880.

(13) Zhou, L.; Xiang, H.-Y.; Shen, S.; Li, Y.-Q.; Chen, J.-D.; Xie, H.-J.; Goldthorpe, I. A.; Chen, L.-S.; Lee, S.-T.; Tang, J.-X. High-Performance Flexible Organic Light-Emitting Diodes Using Embedded Silver Network Transparent Electrodes. *ACS Nano* **2014**, *8*, 12796.

(14) Ellmer, K. Past Achievements and Future Challenges in the Development of Optically Transparent Electrodes. *Nat. Photonics* **2012**, *6*, 809.

(15) Wang, Z.; Nayak, P. K.; Caraveo-Frescas, J. A.; Alshareef, H. N. Recent Developments in P-Type Oxide Semiconductor Materials and Devices. *Adv. Mater.* **2016**, *28*, 3831.

(16) Zhang, K. H. L.; Wu, R.; Tang, F.; Li, W.; Oropeza, F. E.; Qiao, L.; Lazarov, V. K.; Du, Y.; Payne, D. J.; MacManus-Driscoll, J. L.; Blamire, M. G. Electronic Structure and Band Alignment at the NiO and SrTiO₃ p−n Heterojunctions. *ACS Appl. Mater. Interfaces* **2017**, *9*, 26549.

(17) Zhang, J. Y.; Li, W. W.; Hoye, R. L. Z.; MacManus-Driscoll, J. L.; Budde, M.; Bierwagen, O.; Wang, L.; Du, Y.; Wahila, M. J.; Piper, L. F. J.; Lee, T.-L.; Edwards, H. J.; Dhanak, V. R.; Zhang, K. H. L. Electronic and Transport Properties of Li-doped NiO Epitaxial Thin Films. *J. Mater. Chem. C* **2018**, *6*, 2275.

(18) Mryasov, O. N.; Freeman, A. Electronic Band Structure of Indium Tin Oxide and Criteria for Transparent Conducting Behavior. *Phys. Rev. B: Condens. Matter Mater. Phys.* **2001**, *64*, 233111.

(19) Minami, T. Transparent Conducting Oxide Semiconductors for Transparent Electrodes. *Semicond. Sci. Technol.* **2005**, *20*, S35.

(20) Granqvist, C. G. Transparent Conductors as Solar Energy Materials: A Panoramic Review. *Sol. Energy Mater. Sol. Cells* **2007**, *91*, 1529.

(21) Fortunato, E.; Ginley, D.; Hosono, H.; Paine, D. C. Transparent Conducting Oxides for Photovoltaics. *MRS Bull.* **2007**, *32*, 242.

(22) Zhao, R.; Chen, Y.; Ji, Y.; Li, W.; Chen, L.; He, A.; Lu, H.; Zhao, M.; Yao, J.; Jiang, Y.; Liu, G.; Gao, J.; Wang, H.; Yang, H. Controllable Conduction and Hidden Phase Transitions Revealed via Vertical Strain. *Appl. Phys. Lett.* **2019**, *114*, 252901.

(23) Li, W.; Gu, J.; He, Q.; Zhang, K. H. L.; Wang, C.; Jin, K.; Wang, Y.; Acosta, M.; Wang, H.; Borisevich, A. Y.; MacManus-Driscoll, J. L.; Yang, H. Oxygen-Vacancy-Mediated Dielectric Property in Perovskite $Eu_{0.5}Ba_{0.5}TiO_{3-\delta}$ Epitaxial Thin Films. *Appl. Phys. Lett.* **2018**, *112*, 182906.

(24) Li, W.; He, Q.; Wang, L.; Zeng, H.; Bowlan, J.; Ling, L.; Yrotski, D.; Prasankumar, R.; Zhang, W.; Zhao, R.; Dai, J.; Gu, J.; Shen, S.; Guo, H.; Pi, L.; Wang, H.; Wang, Y.; Ivan, V.-D.; Wu, Y.; Hu, Z.; Chen, B.; Li, R.-W.; Sun, Y.; Jin, K.; Zhang, Y.; Chen, H.-T.; Ju, S.; Andreas, R.; Borisevich, A. Y.; Yang, H. Manipulating Multiple Order Parameters via Oxygen Vacancies: The Case of $Eu_{0.5}Ba_{0.5}TiO_{3-\delta}$. *Phys. Rev. B* **2017**, *96*, 115105.

(25) Zhang, L.; Zhou, Y.; Guo, L.; Zhao, W.; Barnes, A.; Zhang, H.-T.; Eaton, C.; Zheng, Y.; Brahlek, M.; Haneef, H. F.; Podraza, N. J.; Chan, M. H. W.; Gopalan, V.; Rabe, K. M.; Engel-Herbert, R. Correlated Metals as Transparent Conductors. *Nat. Mater.* **2016**, *15*, 204.

(26) Hicks, C. W.; Gibbs, A. S.; Mackenzie, A. P.; Takatsu, H.; Maeno, Y.; Yelland, E. A. Quantum Oscillations and High Carrier Mobility in the Delafossite $PdCoO_2$. *Phys. Rev. Lett.* **2012**, *109*, 116401.

(27) Li, C.-I.; Lin, J.-C.; Liu, H.-J.; Chu, M.-W.; Chen, H.-W.; Ma, C.-H.; Tsai, C.-Y.; Huang, H.-W.; Lin, H.-J.; Liu, H.-L.; Chiu, P.-W.; Chu, Y.-H.; Chu, Y. H. Van der Waal Epitaxy of Flexible and Transparent VO_2 Film on Muscovite. *Chem. Mater.* **2016**, *28*, 3914.

(28) Moyer, J. A.; Eaton, C.; Engel-Herbert, R. Highly Conductive $SrVO_3$ as A Bottom Electrode for Functional Perovskite Oxides. *Adv. Mater.* **2013**, *25*, 3578.

(29) Xu, R.; Ji, Y.; Bouchilaoun, R.; Qian, F.; Li, M.; Zhang, X.; Tang, R.; Zhao, R.; Misra, S.; Wang, H.; Li, W.; Kan, C.; Shi, D.; Fan, J.; Yang, H. Optical and Electrical Properties of (111)-Oriented Epitaxial $SrVO_3$ Thin Films. *Ceram. Int.* **2019**, *45*, 11304.

(30) Mirjolet, M.; Sánchez, F.; Fontcuberta, J. High Carrier Mobility, Electrical Conductivity, and Optical Transmittance in Epitaxial $SrVO_3$ Thin Films. *Adv. Funct. Mater.* **2019**, *29*, 1808432.

(31) Liu, M.; Johnston, M. B.; Snaith, H. J. Efficient Planar Heterojunction Perovskite Solar Cells by Vapour Deposition. *Nature* **2013**, *501*, 395.

(32) Green, M. A.; Ho-Baillie, A.; Snaith, H. J. The Emergence of Perovskite Solar Cells. *Nat. Photonics* **2014**, *8*, 506.

(33) Jeon, N. J.; Noh, J. H.; Yang, W. S.; Kim, Y. C.; Ryu, S.; Seo, J.; Seok, S. I. Compositional Engineering of Perovskite Materials for High-Performance. *Nature* **2015**, *517*, 476.

(34) Zhao, Y.; Zhu, K. Organic−Inorganic Hybrid Lead Halide Perovskites for Optoelectronic and Electronic Applications. *Chem. Soc. Rev.* **2016**, *45*, 655.

(35) Tian, W.; Zhou, H.; Li, L. Hybrid Organic−Inorganic Perovskite Photodetectors. *Small* **2017**, *13*, 1702107.

(36) Deng, H.; Yang, X.; Dong, D.; Li, B.; Yang, D.; Yuan, S.; Qiao, K.; Cheng, Y.-B.; Tang, J.; Song, H. Flexible and Semitransparent Organolead Triiodide Perovskite Network Photodetector Arrays with High Stability. *Nano Lett.* **2015**, *15*, 7963.

(37) Hu, X.; Zhang, X.; Liang, L.; Bao, J.; Li, S.; Yang, W.; Xie, Y. High-Performance Flexible Broadband Photodetector Based on Organolead Halide Perovskite. *Adv. Funct. Mater.* **2014**, *24*, 7373.

(38) Cardona, M. Optical Properties and Band Structure of $SrTiO_3$ and $BaTiO_3$. *Phys. Rev.* **1965**, *140*, A651.

(39) Capizzi, M.; Frova, A. Optical Gap of Strontium Titanate (deviation from Urbach tail behavior). *Phys. Rev. Lett.* **1970**, *25*, 1298.

(40) Deepa, M.; Salado, M.; Calio, L.; Kazim, S.; Shivaprasad, S. M.; Ahmad, S. Cesium Power: Low Cs+ Levels Impart Stability to Perovskite Solar Cells. *Phys. Chem. Chem. Phys.* **2017**, *19*, 4069.

(41) Wang, M.; Cao, F. R.; Deng, K. M.; Li, L. Adduct Phases Induced Controlled Crystallization for Mixed-Cation Perovskite Solar Cells with Efficiency Over 21%. *Nano Energy* **2019**, *63*, 103867.

(42) Jeon, Y. P.; Woo, S. J.; Kim, T. W. Transparent and Flexible Photodetectors Based on $CH_3NH_3PbI_3$ Perovskite Nanoparticles. *Appl. Surf. Sci.* **2018**, *434*, 375.

(43) Deng, H.; Dong, D.; Qiao, K.; Bu, L.; Li, B.; Yang, D.; Wang, H.-E.; Cheng, Y.; Zhao, Z.; Tang, J.; Song, H. Growth, Patterning and Alignment of Organolead Iodide Perovskite Nanowires for Optoelectronic Devices. *Nanoscale* **2015**, *7*, 4163.

(44) Dong, R.; Fang, Y.; Chae, J.; Dai, J.; Xiao, Z.; Dong, Q.; Yuan, Y.; Centrone, A.; Zeng, X. C.; Huang, J. High-Gain and Low-Driving-Voltage Photodetectors Based on Organolead Triiodide Perovskites. *Adv. Mater.* **2015**, *27*, 1912.

(45) Lu, H.; Tian, W.; Cao, F.; Ma, Y.; Gu, B.; Li, L. A Self-Powered and Stable All-Perovskite Photodetector−Solar Cell Nanosystem. *Adv. Funct. Mater.* **2016**, *26*, 1296.

(46) Adinolfi, V.; Ouellette, O.; Saidaminov, M. I.; Walters, G.; Abdelhady, A. L.; Bakr, O. M.; Sargent, E. H. Fast and Sensitive Solution-Processed Visible-Blind Perovskite UV Photodetectors. *Adv. Mater.* **2016**, *28*, 7264.

(47) Maculan, G.; Sheikh, A. D.; Abdelhady, A. L.; Saidaminov, M. I.; Haque, M. A.; Murali, B.; Alarousu, E.; Mohammed, O. F.; Wu, T.; Bakr, O. M. $CH_3NH_3PbCl_3$ Single Crystals: Inverse Temperature Crystallization and Visible-Blind UV-Photodetector. *J. Phys. Chem. Lett.* **2015**, *6*, 3781.

(48) Saidaminov, M.; Adinolfi, V.; Comin, R.; Abdelhady, A.; Peng, W.; Dursun, I.; Yuan, M.; Hoogland, S.; Sargent, E. Planar-Integrated Single-Crystalline Perovskite Photodetectors. *Nat. Commun.* **2015**, *6*, 8724.

(49) Li, C.; Han, C.; Zhang, Y.; Zang, Z.; Wang, M.; Tang, X.; Du, J. Enhanced Photoresponse of Self-Powered Perovskite Photodetector Based on ZnO Nanoparticles Decorated $CsPbBr_3$ Films. *Sol. Energy Mater. Sol. Cells* **2017**, *172*, 341.

(50) Leung, S.-F.; Ho, K.-T.; Kung, P.-K.; Hsiao, V. K. S.; Alshareef, H. N.; He, J.-H.; H, J.-H. A Self-Powered and Flexible Organometallic Halide Perovskite Photodetector with Very High Detectivity. *Adv. Mater.* **2018**, *30*, 1704611.

(51) Bao, C.; Zhu, W.; Yang, J.; Li, F.; Gu, S.; Wang, Y.; Yu, T.; Zhu, J.; Zhou, Y.; Zou, Z. Highly Flexible Self-Powered Organolead Trihalide Perovskite Photodetectors with Gold Nanowire Networks as Transparent Electrodes. *ACS Appl. Mater. Interfaces* **2016**, *8*, 23868−23875.

(52) Wang, Y.; Zhang, X.; Wang, D.; Li, X.; Meng, J.; You, J.; Yin, Z.; Wu, J. Compositional Engineering of Mixed-Cation Lead Mixed-Halide Perovskites for High-Performance Photodetectors. *ACS Appl. Mater. Interfaces* **2019**, *11*, 28005−28012.

(53) Cao, F.; Tian, W.; Wang, M.; Cao, H.; Li, L. Semitransparent, Flexible, and Self-Powered Photodetectors Based on Ferroelectricity-Assisted Perovskite Nanowire Arrays. *Adv. Funct. Mater.* **2019**, *29*, 1901280.